WATER RESOURCES RESEARCH, VOL. 29, NO. 7, PAGES 2399–2413, JULY 1993

A Finite-Volume Eulerian-Lagrangian Localized Adjoint Method for Solution of the Advection-Dispersion Equation

R. W. HEALY

U.S. Geological Survey, Denver, Colorado

T. F. RUSSELL

Department of Mathematics, University of Colorado, Denver

A new mass-conservative method for solution of the one-dimensional advection-dispersion equation is derived and discussed. Test results demonstrate that the finite-volume Eulerian-Lagrangian localized adjoint method (FVELLAM) outperforms standard finite-difference methods, in terms of accuracy and efficiency, for solute transport problems that are dominated by advection. For dispersion-dominated problems, the performance of the method is similar to that of standard methods. Like previous ELLAM formulations, FVELLAM systematically conserves mass globally with all types of boundary conditions. FVELLAM differs from other ELLAM approaches in that integrated finite differences, instead of finite elements, are used to approximate the governing equation. This approach, in conjunction with a forward tracking scheme, greatly facilitates mass conservation. The mass storage integral is numerically evaluated at the current time level, and quadrature points are then tracked forward in time to the next level. Forward tracking permits straightforward treatment of inflow boundaries, thus avoiding the inherent problem in backtracking, as used by most characteristic methods, of characteristic lines intersecting inflow boundaries. FVELLAM extends previous ELLAM results by obtaining mass conservation locally on Lagrangian space-time elements. Details of the integration, tracking, and boundary algorithms are presented. Test results are given for problems in Cartesian and radial coordinates.

INTRODUCTION

The advection-dispersion equation (ADE) describes the movement of miscible fluids and is widely used in several different scientific fields. Hydrologists use the ADE to describe the transport of solutes in groundwater and surface water. It is also used by atmospheric physicists to describe the movement of aerosols and trace gases in the atmosphere. In general, there are few applications for which there exists an analytical solution to the ADE. Therefore it is common to rely on numerical solutions to the ADE to predict solute movement. The most common solutions are based on the finite-difference methods (FDM) or finite-element methods (FEM).

While FDM and FEM solutions work well for problems of solute transport that are dominated by dispersive movement, they are limited by two problems for transport problems that are dominated by advective movement: numerical dispersion and oscillation. Numerical dispersion, common in first-order schemes, is the smearing of sharp solute concentration fronts. In terms of results of numerical simulations, numerical dispersion gives the appearance of an artificial, grid-dependent increase in physical dispersion. Numerical oscillation, common in second-order schemes, is manifested by overshoot and undershoot about the true solution. Both of these problems can be resolved by the use of refined space and time grids; however, the added computational effort needed to reach the required degree of refinement commonly makes a simulation intractable for most computers. Many attempts have been made to develop alternative techniques to efficiently solve advection-dominated problems. Recent developments have generally been along one of two approaches: Eulerian or characteristic methods. Eulerian methods use a fixed spatial grid. Included in this class are optimal spatial methods [*Brooks and Hughes*, 1982] that attempt to minimize the error in approximating spatial derivatives. These methods make use of upstream weighting and hence are susceptible to time truncation errors, which introduce numerical dispersion, and limitations on the size of the Courant number (usually less than 1). *Bouloutas and Celia* [1988] present a comparison of several optimal spatial methods. For advection-dominated problems, such methods generally require small time steps for reasons of accuracy, even if they are implicit and therefore stable with large time steps. This is because the time truncation error depends on high-order time derivatives of concentration, which are large when a moving front passes by. Other Eulerian methods, such as the Petrov-Galerkin FEM of *Westerink and Shea* [1989] and the total variation diminishing scheme of *Cox and Nishikawa* [1991], attempt to reduce the overall truncation error by using spatial errors to cancel temporal errors. Here the temporal discretization introduces negative numerical dispersion to cancel the positive spatial numerical dispersion, so these methods suffer from restrictions on the Courant number.

Characteristic methods solve separately for the advective and dispersive components of the ADE. Advection is solved on a Lagrangian-type grid by tracking along characteristics of the velocity field. Dispersion is solved on an Eulerian spatial grid. Many approaches to characteristic methods have appeared in the literature under a variety of names, including Eulerian-Lagrangian methods [*Neuman*, 1981, 1984], method of characteristics [*Garder et al.*, 1964; *Koni-*

Paper number 93WR00403.
0043-1397/93/93WR-00403$05.00

kow and Bredehoeft, 1978], modified method of characteristics [*Douglas and Russell*, 1982; *Russell*, 1985; *Russell et al.*, 1986], and operator-splitting methods [*Espedal and Ewing*, 1987; *Dahle et al.*, 1988]. These approaches have greatly improved time truncation errors compared to standard FDM and FEM or Eulerian methods. Therefore large time step sizes may be taken with little loss of accuracy. Problems with characteristic methods, in general, arise in three areas: inability to rigorously treat boundary fluxes when characteristics intersect inflow or outflow boundaries, inability to ensure conservation of mass, and the introduction of numerical dispersion, for some methods, due to low-order interpolation or integration [*Healy and Russell*, 1989]. The mass conservation problem is due to the aforementioned boundary problem and the use of the nondivergence form of the ADE. With the nondivergence form, errors in the velocity field and in tracking of characteristics result in errors in mass conservation. The Eulerian-Lagrangian localized adjoint method (ELLAM) of *Celia et al.* [1990] and *Russell* [1990] presents a consistent framework for treating boundary fluxes and guaranteeing mass conservation in a finite-element approach.

This paper presents details of development and implementation of a finite-volume Eulerian-Lagrangian localized adjoint method (FVELLAM). FVELLAM is an extension of the work of *Celia et al.* [1990] to an integrated finite-difference setting. The new method shares some advantages of ELLAM such as consistent treatment of boundaries and global mass conservation. In addition, FVELLAM obtains local mass conservation on Lagrangian space-time control volumes and makes the ELLAM framework more convenient for existing solute transport codes that are based on finite volumes or body-centered finite differences. Like ELLAM, FVELLAM has the capability to treat problems with variable coefficients (due to variable velocity field or variable spacing). The methodology by which this is accomplished is discussed. The utility of the program is demonstrated with two example problems, the results of which are compared to those of standard FDM and analytical solutions. Limitations of the approach and extension to multiple dimensions are also discussed.

METHODS

Derivation of Equations

The one-dimensional advection-dispersion equation, under conditions of uniform porosity and incompressible fluid and media, can be written along with appropriate initial and boundary conditions as

$$Lc \equiv \frac{\partial c(x,\,t)}{\partial t} + \frac{\partial}{\partial x}\left(v(x,\,t)c(x,\,t) - D\,\frac{\partial c(x,\,t)}{\partial x}\right) = f(x,\,t), \qquad x \in [0,\,l] = \Omega \qquad t \in [0,\,T] \tag{1}$$

$$c(x,\,0) = c_0(x), \qquad c(x,\,t) = h(x,\,t),$$

or

$$-D\,\frac{\partial c(x,\,t)}{\partial x} = h(x,\,t),$$

or

$$v(x,\,t)c(x,\,t) - D\,\frac{\partial c(x,\,t)}{\partial x} = h(x,\,t) \qquad x = 0,\ x = l$$

Eulerian-Lagrangian localized adjoint methods consider the weak form of (1) obtained by integration against the space-time test function $w(x,\,t)$:

$$\int_0^T \int_0^l (Lc - f)w\,dx\,dt = 0 \tag{2}$$

Substituting (1) into (2) and noting that

$$\frac{\partial c}{\partial t}\,w = \frac{\partial (cw)}{\partial t} - c\,\frac{\partial w}{\partial t},$$

$$\frac{\partial}{\partial x}\left(vc - D\,\frac{\partial c}{\partial x}\right)w = \frac{\partial}{\partial x}\left(\left(vc - D\,\frac{\partial c}{\partial x}\right)w\right) - \left(vc - D\,\frac{\partial c}{\partial x}\right)\frac{\partial w}{\partial x}$$

we can write:

$$\int_0^l \int_0^T \frac{\partial (c(x,\,t)w(x,\,t))}{\partial t}\,dt\,dx + \int_0^T \int_0^l \cdot \frac{\partial}{\partial x}\left[\left(v(x,\,t)c(x,\,t) - D\,\frac{\partial c}{\partial x}\,(x,\,t)\right)w(x,\,t)\right]dx\,dt + \int_0^T \int_0^l D\,\frac{\partial c}{\partial x}\,(x,\,t)\,\frac{\partial w}{\partial x}\,(x,\,t)\,dx\,dt - \int_0^T \int_0^l c\left(\frac{\partial w}{\partial t}\,(x,\,t) + v(x,\,t)\,\frac{\partial w}{\partial x}\,(x,\,t)\right)dx\,dt = \int_0^T \int_0^l f(x,\,t)w(x,\,t)\,dxdt \tag{3}$$

The term $(\partial w/\partial t) + v(\partial w/\partial x)$ appearing in the fourth integral on the left-hand side is the adjoint associated with the hyperbolic part of L. We first divide time into discrete intervals $[t^n,\,t^{n+1}]$ such that $\Delta t = t^{n+1} - t^n$ and require that c be continuous on each time interval. In addition, $w(x,\,t)$ must vanish for $t \notin [t^n,\,t^{n+1}]$. Equation (3) can then be rewritten

$$\int_0^l c(x,\,t^{n+1})w(x,\,t^{n+1})\,dx + \int_{t^n}^{t^{n+1}} \int_{\partial\Omega} \cdot \left[v(x,\,t)c(x,\,t) - D\,\frac{\partial c(x,\,t)}{\partial x}\right] \cdot n(x)w(x,\,t)\,dS\,dt + \int_{t^n}^{t^{n+1}} \int_0^l D\,\frac{\partial c(x,\,t)}{\partial x}\,\frac{\partial w(x,\,t)}{\partial x}\,dx\,dt - \int_{t^n}^{t^{n+1}} \int_0^l c(x,\,t)\left(\frac{\partial w(x,\,t)}{\partial t} + v(x,\,t)\,\frac{\partial w(x,\,t)}{\partial x}\right)dx\,dt$$

$$= \int_0^l c(x, t^n)w(x, t^n)\, dx$$

$$+ \int_{t^n}^{t^{n+1}} \int_0^l f(x, t)w(x, t)\, dx\, dt, \qquad (4)$$

where Green's formula has been employed to transform the second integral on the left-hand side to an integral over the domain boundary $\partial\Omega$, and $n(x)$ is the outward unit normal on $\partial\Omega$. In the one-dimensional case, $\partial\Omega$ consists of the two points 0 and l, with $n(0) = -1$ and $n(l) = 1$. That integral now represents boundary fluxes and will be nonzero only near boundaries.

We next divide the spatial domain into intervals or finite volumes $[x_{i-(1/2)}, x_{i+(1/2)}]$ of length Δx_i, with node x_i at the center; thus, $x_{i\pm(1/2)} = x_i \pm (\Delta x_i/2)$. With each finite volume we associate a test function $w_i(x, t)$, which we now define.

Given a point $(\bar{x}, \bar{t})$, with $\bar{t} \in [t^n, t^{n+1}]$, we consider the ordinary differential equation $x'(t) = v(x(t), t)$, $x(\bar{t}) = \bar{x}$, that tracks the advective flow from $(\bar{x}, \bar{t})$. Denote the solution of this equation at time t, $x(t)$, by $X(t; \bar{x}, \bar{t})$. This notation can refer to tracking forward or backward in time; in particular, we define

$$x^* = X(t^n; x, t^{n+1}),$$
$$\hat{x} = X(t^{n+1}; x, t^n), \qquad (5)$$

so that (x, t^{n+1}) backtracks to (x^*, t^n) and (x, t^n) tracks forward to $(\hat{x}, t^{n+1})$. The interval $[x^*_{i-(1/2)}, x^*_{i+(1/2)}]$, illustrated in Figure 1, tracks forward to the finite volume $[x_{i-(1/2)}, x_{i+(1/2)}]$. The ELLAM method selects $w(x, t)$ so as to make the adjoint integral of $(\partial w/\partial t) + v(\partial w/\partial x)$ vanish for all x and t; thus, we seek $w(x, t)$ that is constant along flow lines. At time t^{n+1}, it is natural to ask that $w_i(x, t^{n+1})$ be 1 in the finite volume $[x_{i-(1/2)}, x_{i+(1/2)}]$ and 0 outside. Hence, we define

$$w_i(x, t) = 1 \qquad X(t^{n+1}; x, t) \in [x_{i-(1/2)}, x_{i+(1/2)}], \quad t \in [t^n, t^{n+1}]$$
$$w_i(x, t) = 0 \qquad \text{otherwise} \qquad (6)$$

At time t^n, we see that $w_i(x, t^n)$ is 1 if $x \in [x^*_{i-(1/2)}, x^*_{i+(1/2)}]$ and 0 otherwise. In Figure 1, $w_i(x, t)$ would be 1 inside the parallelogram and 0 outside.

Noting that $\partial w_i/\partial x(x, t^{n+1})$ is now a delta function at $x_{i-(1/2)}$ and $x_{i+(1/2)}$, a one-step backward Euler approximation at t^{n+1} to the time integrals in (4) results in the following

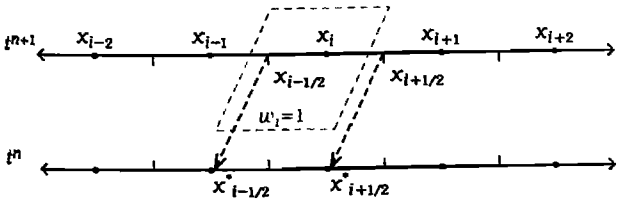

Fig. 1. Spatial grid with characteristic lines.

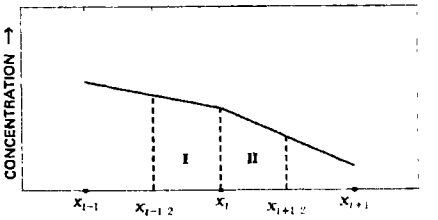

Fig. 2. Concentration as linear function of distance between nodes, showing the applicability of the trapezoid rule with two subintervals (I and II).

equation for interior cells that are not affected by boundary fluxes:

$$\int_{x_{i-(1/2)}}^{x_{i+(1/2)}} c(x, t^{n+1})\, dx + D\Delta t\left[\frac{\partial c}{\partial x}(x_{i-(1/2)}, t^{n+1}) - \frac{\partial c}{\partial x}(x_{i+(1/2)}, t^{n+1})\right]$$
$$= \int_{x^*_{i-(1/2)}}^{x^*_{i+(1/2)}} c(x, t^n)\, dx + \Delta t \int_{x_{i-(1/2)}}^{x_{i+(1/2)}} f(x, t^{n+1})\, dx \qquad (7)$$

The boundary flux integral is addressed in detail in subsequent sections.

Previous ELLAM simulations have been limited to a finite-element approach. Here, (7) is solved with an integrated finite-difference approach. We believe this approach is beneficial for the following reasons. First, there are many widely used finite-difference flow and solute transport models in both the groundwater and oil industries today. Modifications of such codes to incorporate the FVELLAM is likely to be more cost-effective than completely rewriting finite-difference codes to use the finite-element ELLAM. Second, we believe that our approach may have some advantages over the FEM in treatment of variable coefficients and boundary fluxes. Finally, by defining the test function w_i as above, we are able to conserve mass locally on the Lagrangian elements described by $[x_{i-(1/2)}, x_{i+(1/2)}]$ and $[t^n, t^{n+1}]$ and shown in Figure 1.

The integrals in (7), with the exception of the first integral on the right-hand side, are approximated by standard numerical integration techniques.

The spatial derivatives of concentration are approximated by assuming that concentration varies linearly in space between adjacent nodes. Typically, finite-volume methods lump the storage integrals, i.e., they assume that concentration is piecewise constant within each cell. We found that this approach introduced unacceptable levels of numerical dispersion into results for some problems. Hence it was decided to again assume a linear variation in concentration in order to evaluate these integrals. This leads to a scheme that combines Lagrangian aspects with control volume finite-element approaches of earlier authors [e.g., *Baliga and Patankar*, 1980; *Liu and McCormick*, 1988; *Forsyth*, 1989; *Heinemann et al.*, 1989; *Rozon*, 1989]. The trapezoid rule is then exact for the first integral on the left-hand side of (7). With each cell broken into two trapezoids and three integration points $(x_{i-(1/2)}, x_i, x_{i+(1/2)})$ as shown in Figure 2, we have

$$\int_{x_{i-(1/2)}}^{x_{i+(1/2)}} c(x, t^{n+1})\, dx = \Delta x\left(\frac{1}{8} c_{i-1}^{n+1} + \frac{3}{4} c_i^{n+1} + \frac{1}{8} c_{i+1}^{n+1}\right) \quad (8a)$$

for uniform spacing and

$$\int_{x_{i-(1/2)}}^{x_{i+(1/2)}} c(x, t^{n+1})\, dx = \Delta x_i\left(\frac{1}{4}\frac{\Delta x_i}{\Delta x_{i-1} + \Delta x_i} c_{i-1}^{n+1} + \left(\frac{1}{2} + \frac{1}{4}\left[\frac{\Delta x_{i-1}}{\Delta x_{i-1} + \Delta x_i} + \frac{\Delta x_{i+1}}{\Delta x_i + \Delta x_{i+1}}\right]\right) c_i^{n+1} + \frac{1}{4}\frac{\Delta x_i}{\Delta x_i + \Delta x_{i+1}} c_{i+1}^{n+1}\right) \quad (8b)$$

for variable spacing. For cells that are adjacent to inflow ($i = 1$) and outflow ($i = L$) boundaries, (8) takes the form

$$\int_{x_{1/2}}^{x_{3/2}} c(x, t^{n+1})\, dx = \Delta x\left(\frac{1}{4} c_{1/2}^{n+1} + \frac{5}{8} c_1^{n+1} + \frac{1}{8} c_2^{n+1}\right)$$

for uniform spacing and

$$\int_{x_{1/2}}^{x_{3/2}} c(x, t^{n+1})\, dx = \Delta x_1\left(\frac{1}{4} c_{1/2}^{n+1} + \left(\frac{1}{2} + \frac{1}{4}\frac{\Delta x_2}{\Delta x_1 + \Delta x_2}\right) c_1^{n+1} + \frac{1}{4}\frac{\Delta x_1}{\Delta x_1 + \Delta x_2} c_2^{n+1}\right)$$

for variable spacing;

$$\int_{x_{L-(1/2)}}^{x_{L+(1/2)}} c(x, t^{n+1})\, dx = \Delta x\left(\frac{1}{8} c_{L-1}^{n+1} + \frac{5}{8} c_L^{n+1} + \frac{1}{4} c_{L+(1/2)}^{n+1}\right)$$

for uniform spacing and

$$\int_{x_{L-(1/2)}}^{x_{L+(1/2)}} c(x, t^{n+1})\, dx = \Delta x_L\left(\frac{1}{4}\frac{\Delta x_L}{\Delta x_{L-1} + \Delta x_L} c_{L-1}^{n+1} + \left(\frac{1}{2} + \frac{1}{4}\frac{\Delta x_{L-1}}{\Delta x_{L-1} + \Delta x_L}\right) c_L^{n+1} + \frac{1}{4} c_{L+(1/2)}^{n+1}\right)$$

for variable spacing, where $c_{1/2}$ and $c_{L+(1/2)}$ refer to concentrations at the boundaries; definitions for these variables are given in the discussion of boundary conditions. The corresponding equations for use in a radial coordinate system are given in the appendix.

With suitable choices of integration rules, (7) is identical to the equation solved by the modified method of characteristics (MMOC) [*Douglas and Russell*, 1982]. However, in practice, FVELLAM does not solve this equation. Instead, the storage integral on the right-hand side of (7) is modified. We revert to (4) and make the following approximation:

$$\int_{x_{i-(1/2)}^*}^{x_{i+(1/2)}^*} c(x, t^n)\, dx \approx \int_0^l c(x, t^n) W_i(x, t^n)\, dx \quad (9)$$

where $W_i(x, t)$ is an approximation to $w_i(x, t)$ that is introduced in order to avoid problems that will be discussed in a later section. Note that $W_i(x, t)$ may take on nonzero values for $x \notin [x_{i-(1/2)}, x_{i+(1/2)}]$; hence the limits of integration are changed in (9).

Two approaches can be used to calculate the integral on the right-hand side of (9). The approach commonly used in characteristic methods is to apply a numerical integration rule at time level $n + 1$ using standard values for $W(x, t)$ and backtracking to time level n, where concentrations are known, from $x_{i-(1/2)}$, $x_{i+(1/2)}$ and intermediate integration points. Values for $c(x^*, t^n)$ are then calculated by linear interpolation in x, and the numerical integration is carried out. Complexities arise with this approach when inflow boundaries are intersected during backtracking, and we know of no simple way to ensure mass conservation because the integration points may not be regularly spaced at time level n.

An alternative approach to evaluating the integral in question has recently been put forth by *Russell and Trujillo* [1990]. Here the numerical integration rule is applied at t^n. Integration points, along with the integration weights associated with them, are forward tracked up to time level $n + 1$. For this approach, standard values for $c(x, t^n)$ are used, but values for $W(x, t^n) = W(\hat{x}, t^{n+1})$, where $\hat{x}$ is the location at t^{n+1} obtained when forward tracking from x at t^n, must be obtained through forward tracking. This scheme has the advantage of straightforward mass conservation and avoiding backtracking off of the spatial grid. Forward tracking does encounter the problem of intersecting outflow boundaries during tracking, but this problem can be easily treated. We have adapted this alternative approach for use in FVELLAM.

For the one-dimensional problems considered in this paper and when $v(x, t)$ is of a simple form (e.g., constant or linear in x and t), a third alternative to evaluating the integral in (9) is exact integration. Exact integration uses a backtracking approach and takes advantage of the linear variation in concentration between nodes. Its use for one-dimensional problems has recently been put forth by M. A. Celia (personal communication, 1991). We do not propose this approach here because it is not practical for multidimensional problems; however, exact integration is used for comparison purposes in discussion of computational results.

Regardless of whether a backward or forward tracking approach is used to evaluate the integral in (9), care must be taken when selecting a numerical integration rule. The rule should conserve mass, and the density of integration points must be great enough to faithfully represent any sharp concentration fronts. If the latter condition is not met then numerical dispersion (or possibly oscillation) could enter into the solution.

Integration at Time Level n

Several different numerical techniques were investigated for evaluating the integrals in (9). As long as the selected technique is conservative, then our method will conserve mass (assuming of course that boundaries are also mass

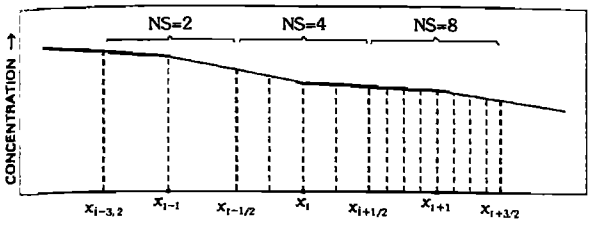

Fig. 3. Location of spatial integration points for NS = 2, 4, and 8.

conservative). Because of the inherent assumption that concentrations vary linearly between adjacent nodes, the obvious choice for integration scheme is again the trapezoid rule (Figure 2). Because of the linearity in c, this method will be exact when $W \equiv 1$, and thus mass will be conserved globally. To calculate the integral, concentrations at integration points that are not nodal locations are determined by linearly interpolating between adjacent nodes.

While the trapezoidal method conserves mass, it became obvious during testing of the method that three integration points per cell were not sufficient to avoid numerical dispersion for all problems. Higher-order integration methods (Simpson and Lobatto-type rules) were investigated to address this problem. However, these methods produced an inconsistency in the difference equation because different formulas were used to represent left- and right-hand side storage integrals in (7), namely, a trapezoidal (exact) integration on the left and a higher-order rule on the right. The net result of this inconsistency was the introduction of negative numerical dispersion, the severity of which was strongly dependent on the cell Peclet number (Pe) and the Courant number (Cr). These matters are covered in detail elsewhere (T. F. Russell and R. W. Healy, manuscript in preparation, 1993). It was decided to use the trapezoid rule, but to increase the number of subintervals within each cell over which the rule is evaluated. The number of subintervals is referred to as NS. The test function W_i will depend on NS in a manner to be described in a later section. A value of 2 for NS corresponds to the original trapezoid rule. Subintervals are equally spaced within each cell, and Figure 3 shows the distributions of subintervals for NS = 2, 4, and 8. Although increasing the value of NS allows for more accurate distribution of mass at time level $n + 1$, it does not affect the accuracy of mass conservation at time level n; values of NS = 2 and NS = 16 produce the same total mass for the integral at time level n. Our experience has shown that a value of 4 for NS was sufficient for solving most problems. As programmed now, the code uses the same number of subintervals for all finite-difference cells in the spatial grid. However, an adaptive approach could be easily incorporated so that finer discretization could automatically be incorporated in the vicinity of sharp fronts. Such a modification will be necessary to make the method practical in multiple dimensions.

Once the number of integration points has been determined, the integral in (9) can be evaluated by

$$\int_0^l c(x, t^n) W_i(x, t^n)\, dx = \sum_{k=1}^{\mathrm{NT}} c(x_k, t^n) U(x_k) W_i(\hat{x}(x_k), t^{n+1}) \qquad (10)$$

where x_k is an integration point, $c(x_k, t^n)$ is determined by linear interpolation, $U(x_k)$ are the integration weights:

$$U(x_k) = \tfrac{1}{2}(x_{k+1} - x_k) \qquad k = 1$$

$$U(x_k) = \tfrac{1}{2}(x_{k+1} - x_{k-1}) \qquad 1 < k < \mathrm{NT}$$

$$U(x_k) = \tfrac{1}{2}(x_k - x_{k-1}) \qquad k = \mathrm{NT}$$

and NT is the total number of integration points.

This method of integration at time level n and forward tracking up to time level $n + 1$ works very well for the case of constant coefficients (i.e., constant grid spacing and velocity). However, for problems involving variable spacing or velocity this approach may fail to properly distribute the integrated mass from t^n to the nodes at t^{n+1}. This problem is manifested by inequality between the sum of the tracked weights $U(x_k)W_i(\hat{x}(x_k), t^{n+1})$ into a particular cell and the total weight (Δx_i) of the cell, or equivalently by inexactness of the integral in (9) when $W \equiv 1$. Essentially, the method attempts to lump more mass into a cell than the cell can contain. This results in a violation of the maximum principle: In the absence of any boundary influence, calculated concentrations for the cell at t^{n+1} may be greater than the concentration at t^n in cells that track into the cell of interest. The resulting concentration field then contains oscillations. This problem can be viewed as a failure to satisfy mass conservation locally in the finite volume $[x_{i-(1/2)}, x_{i+(1/2)}]$ although the global mass balance is not affected.

The severity of this problem can be reduced by simply increasing the number of equally spaced integration points. A more efficient approach is to add integration points at t^n at specific locations. These locations are called strategic space integration points (SSIP). The locations of the SSIPs are determined by backtracking from certain points on the grid from time t^{n+1} to t^n. Further details on determining SSIP locations are presented in a subsequent section. On average there are three SSIPs per grid cell. Since backtracking requires an amount of work identical to forward tracking, inclusion of SSIPs is identical, in terms of work, to increasing NS by 3. Equation (10) requires no modifications to accommodate these new integration points. Inclusion of the SSIPs, in conjunction with selection of an appropriate value for NS, can completely eliminate oscillations from most problems and reduce their severity for particularly stubborn problems to a level where they are of no practical concern.

Tracking

Integration points at time level n are forward tracked according to the second part of (5). For backtracking, the first part is used. To accomplish the tracking, it is assumed that the velocity is known at the intercell boundaries (i.e., $x_{i-(1/2)}, x_{i+(1/2)}, \cdots$) and that velocity is steady in time and varies linearly across each cell. Points are tracked cell by cell using the procedure described by *Pollock* [1988] with the following formula:

$$x_p(t_{j+1}) = x_p(t_j) + (\mathrm{IFB})v(x_p(t_j), t_j) \cdot \{\exp(A\Delta t_{j+1}) - 1\}/A \qquad (11)$$

where $x_p(t_j)$ is the position of the integration point at time t_j; j is an index to time substeps; Δt_j is the length of a time

substep, equal to the time required for a point to be tracked across a complete or partial cell;

$$\sum_{j=1}^{J} \Delta t_j = \Delta t;$$

J is the total number of time substeps; t_j is the time at substep j; $t_0 = t^n$ for forward tracking and t^{n+1} for backtracking; IFB = +1 for forward tracking and −1 for backtracking; and $A = \partial v/\partial x$ for each cell. Equation (11) is inverted to solve for Δt_j so that $x_p(t_{j+1})$ is equal to a cell boundary for all time substeps except the final step.

Selection of Approximate Test Functions

The requirements on the approximate test function $W(x, t)$ are that it must be continuous on the space-time domain in equation (6), be nonzero only on $[t^n, t^{n+1}]$, and satisfy $\sum_i W_i(x, t) = 1$ for $x \in [0, l]$, $t \in [t^n, t^{n+1}]$. There are an infinite number of functions that meet these requirements. The simplest of these functions is given by (6). This form for $W_i(x, t)$ was initially used in our method. Essentially, this form lumps all advected mass into the finite-difference cell in which $\hat{x}$ falls. This function works well for many problems, but when Cr is close to an integer value, results are sensitive to the size of the Courant number. Slight differences in Cr can result in mass's being accumulated in different cells; for example, a problem with a value of $Cr = 1.01$ will result in a faster propagation of a solute front than the same problem with $Cr = 0.99$.

A more general approach to distributing the mass at time level $n + 1$ is to partition the mass among two or more adjacent cells. For a linear distribution of tracked mass, $W_i(x, t)$ takes the form of the familiar "chapeau" function:

$$W_i(\hat{x}, t^{n+1}) = 1 - \frac{x_i - \hat{x}}{x_i - x_{i-1}} \qquad x_{i-1} \le \hat{x} \le x_i$$

$$W_i(\hat{x}, t^{n+1}) = 1 - \frac{\hat{x} - x_i}{x_{i+1} - x_i} \qquad x_i \le \hat{x} \le x_{i+1} \tag{12}$$

$$W_i(\hat{x}, t^{n+1}) = 0 \qquad \hat{x} < x_{i-1} \text{ or } \hat{x} > x_{i+1}$$

For most problems of practical concern, this form of the test function produces excellent results. However, for problems with small Cr and NS > 2, (12) introduces numerical dispersion into the results. That dispersion is particularly apparent at the limiting case of $Cr = 0$. The desire to insure no numerical dispersion for this case motivated development of the following form of the test function, which is implemented in our method:

$$W_i(\hat{x}, t^{n+1}) = 0 \qquad \hat{x} < x_{i-(1/2)} - \overline{\Delta x}_{i-1} \tag{13a}$$

$$W_i(\hat{x}, t^{n+1}) = \frac{\Delta x_i}{\Delta x_{i-1} + \Delta x_i}\left(1 - \frac{x_{i-(1/2)} - \hat{x}}{\overline{\Delta x}_{i-1}}\right) \tag{13b}$$

$$x_{i-(1/2)} - \overline{\Delta x}_{i-1} \le \hat{x} \le x_{i-(1/2)}$$

$$W_i(\hat{x}, t^{n+1}) = \frac{\Delta x_i + (\hat{x} - x_{i-(1/2)})\Delta x_{i-1}/\overline{\Delta x}_i}{\Delta x_{i-1} + \Delta x_i} \tag{13c}$$

$$x_{i-(1/2)} \le \hat{x} \le x_{i-(1/2)} + \overline{\Delta x}_i$$

$$W_i(\hat{x}, t^{n+1}) = 1 \qquad x_{i-(1/2)} + \overline{\Delta x}_i \le \hat{x} \le x_{i+(1/2)} - \overline{\Delta x}_i \tag{13d}$$

$$W_i(\hat{x}, t^{n+1}) = \frac{\Delta x_i + (x_{i+(1/2)} - \hat{x})\Delta x_{i+1}/\overline{\Delta x}_i}{\Delta x_i + \Delta x_{i+1}} \tag{13e}$$

$$x_{i+(1/2)} - \overline{\Delta x}_i \le \hat{x} \le x_{i+(1/2)}$$

$$W_i(\hat{x}, t^{n+1}) = \frac{\Delta x_i}{\Delta x_i + \Delta x_{i+1}}\left(1 - \frac{\hat{x} - x_{i+(1/2)}}{\overline{\Delta x}_{i+1}}\right) \tag{13f}$$

$$x_{i+(1/2)} \le \hat{x} \le x_{i+(1/2)} + \overline{\Delta x}_{i+1}$$

$$W_i(\hat{x}, t^{n+1}) = 0 \qquad \hat{x} > x_{i+(1/2)} + \overline{\Delta x}_{i+1} \tag{13g}$$

where $\overline{\Delta x}_i = \Delta x_i/\text{NS}$, $i = 2$ to $L - 1$, and L is the total number of finite-difference cells. For cells that are adjacent to boundaries ($i = 1$ for $x = 0$ and $i = L$ for $x = l$) equations (13) require slight modifications. When $i = 1$, (13*b*)–(13*d*) are replaced by

$$W_1(\hat{x}, t^{n+1}) = 1 \qquad 0 \le \hat{x} \le x_{3/2} - \overline{\Delta x}_1, \tag{13h}$$

and when $i = L$, (13*d*)–(13*f*) are replaced by

$$W_L(\hat{x}, t^{n+1}) = 1 \qquad x_{L-(1/2)} + \overline{\Delta x}_L \le \hat{x} \le l. \tag{13i}$$

Substitution of (13) into (10) produces an equation identical in form to (8) on the right-hand side.

Test functions are illustrated at t^{n+1} for a uniform spatial grid in Figure 4 for NS = 2, 4, and 8; and for a nonuniform grid with NS = 4. Discussion of the approximate test functions used for a radial coordinate system is given in the appendix. For NS = 2, (13) reduces to (12). It is interesting to note in Figure 4*b* that $W_{i-1}(x_{i-(1/2)}, t^{n+1})$ is less than $W_i(x_{i-(1/2)}, t^{n+1})$, even though $x_{i-(1/2)}$ is closer to x_{i-1} than to x_i.

It is now possible to fully describe the location of the SSIPs. The SSIPs are obtained by backtracking from the points on the grid where the slope of the test function changes. There are three such points in each cell i: $x_{i-(1/2)}$, $x_{i-(1/2)} + \overline{\Delta x}_i$, and $x_{i+(1/2)} - \overline{\Delta x}_i$. These points are backtracked from time level $n + 1$ to level n and then incorporated into the numerical integration scheme. Because the tracked location of the SSIPs at time level $n + 1$ is known, there is no need to forward track these points along with the other integration points.

Inflow Boundaries

Inflow boundaries come into play when a spatial boundary is intersected at time $t^*_{i-(1/2)} > t_n$ when backtracking along the characteristic curve from $x_{i-(1/2)}$ at t^{n+1} (Figure 5). When this occurs, (7) must be modified, as the boundary flux integral is now nonzero:

$$\int_{x_{i-(1/2)}}^{x_{i+(1/2)}} c(x, t^{n+1})\, dx$$

$$+ D\left[(t^{n+1} - t^*_{i-(1/2)})\frac{\partial c}{\partial x}(x_{i-(1/2)}, t^{n+1})\right.$$

$$- \Delta t \frac{\partial c}{\partial x}(x_{i+(1/2)}, t^{n+1})\Bigg]$$

$$+ \int_{t^n}^{t^{n+1}} \int_{\partial\Omega} \left[v(x, t)c(x, t) - D \frac{\partial c}{\partial x} \right] \cdot n(x) W_i(x, t)\, dS\, dt = \int_0^l c(x, t^n) W_i(x, t^n)\, dx$$

$$+ \int_{x_{i-(1/2)}}^{x_{i+(1/2)}} f(x, t^{n+1}) \Delta t(x)\, dx \qquad (14)$$

where $\Delta t(x)$ is the time in which x backtracks to the boundary; thus $\Delta t(x_{i-(1/2)}) = t^{n+1} - t^*_{i-(1/2)}$ and $\Delta t(x) = \Delta t$ if x does not backtrack to the boundary.

The approximate test function $W(x, t)$ has been inserted into the boundary flux integral. In the case where backtracking from $x_{i+(1/2)}$ at t^{n+1} also intersects the boundary (at $t^*_{i+(1/2)}$), then Δt is replaced by $t^{n+1} - t^*_{i+(1/2)}$ in the dispersion term and the first integral on the right-hand side of the equation vanishes. With the exception of the boundary flux integral, all terms in (14) are treated as previously described.

Dirichlet condition. The boundary flux integral for the Dirichlet condition becomes

$$-\left(\int_{t^n}^{t^{n+1}} h(0, t) W_i(\hat{X}, t^{n+1}) v(0, t)\, dt - \int_{t^n}^{t^{n+1}} D \frac{\partial c}{\partial x}(0, t) W_i(\hat{X}, t^{n+1})\, dt \right) \qquad (15)$$

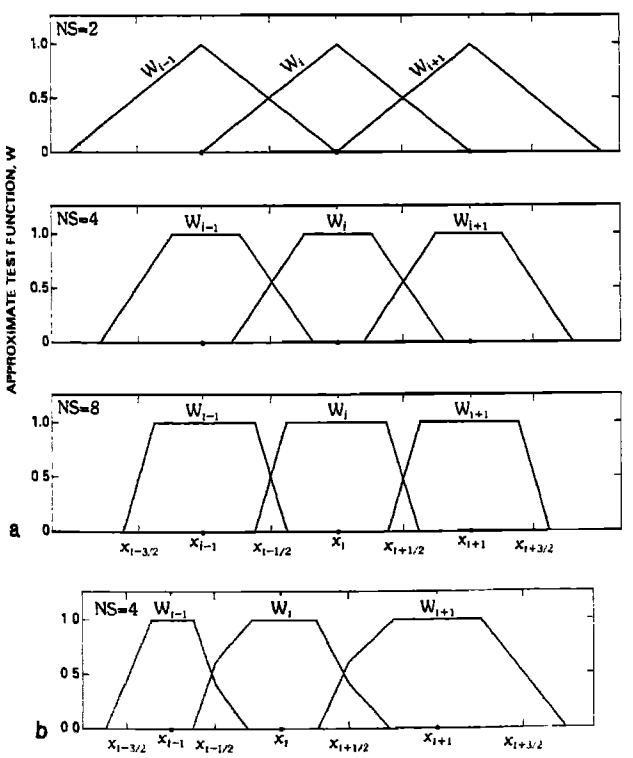

Fig. 4. Approximate test functions at t^{n+1}: (*a*) NS = 2, 4, and 8 for uniform grid; (*b*) NS = 4 for nonuniform grid.

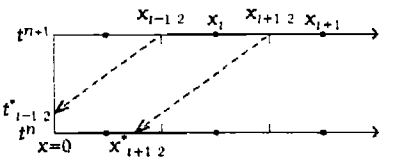

Fig. 5. Characteristic line intersecting inflow boundary when backtracking for time level $n + 1$.

where $\hat{X}(t) = X(t^{n+1}; 0, t)$ is now the forward tracked point in space at time t^{n+1} starting from time t at $x = 0$, the inflow boundary is at $x = 0$, and $h(x, t)$ is the boundary data function in (1). The dispersion integral is approximated by an integral over $[x_{i-(1/2)}, x_{i+(1/2)}]$ at t^{n+1}, using $dt = (1/v)\, dx$, and the resulting terms are incorporated into the implicit solution of (7). The dispersive boundary flux can then be calculated. The advective boundary flux term is treated by numerical integration in time and forward tracking of the integration points in time from the boundary onto the spatial grid. We again use the trapezoid rule to evaluate the integral. Intermediate time integration points may be included between t^n and t^{n+1} and are denoted by t^*_k where

$$t^*_0 = t^n$$
$$t^*_{k-1} < t^*_k \qquad 1 \le k \le K \qquad (16)$$
$$t^*_K = t^{n+1},$$

and $K + 1$ is the number of time integration points.

We can then write

$$\int_{t^n}^{t^{n+1}} h(0, t) v(0, t) W_i(\hat{X}, t^{n+1})\, dt = \sum_{k=1}^{K} \int_{t^*_{k-1}}^{t^*_k} h(0, t) v(0, t) W_i(\hat{X}, t^{n+1})\, dt \qquad (17)$$

Applying the trapezoid rule produces

$$\int_{t^*_{k-1}}^{t^*_k} h(0, t) v(0, t) W_i(\hat{X}, t^{n+1})\, dt = \frac{1}{2}(t^*_k - t^*_{k-1}) \cdot [h(0, t^*_k) v(0, t^*_k) W_i(X(t^{n+1}; 0, t^*_k), t^{n+1}) + h(0, t^*_{k-1}) v(0, t^*_{k-1}) W_i(X(t^{n+1}; 0, t^*_{k-1}), t^{n+1})] \qquad (18)$$

$$\sum_{k=1}^{K} \int_{t^*_{k-1}}^{t^*_k} h(0, t) v(0, t) W_i(\hat{X}, t^{n+1})\, dt = \frac{1}{2} \Bigg\{ \sum_{k=1}^{K-1} (t^*_{k+1} - t^*_{k-1}) h(0, t^*_k) v(0, t^*_k) W_i(X(t^{n+1}; 0, t^*_k), t^{n+1}) + (t^*_1 - t^*_0) h(0, t^*_0) v(0, t^*_0) W_i(X(t^{n+1}; 0, t^*_0), t^{n+1}) + (t^*_K - t^*_{K-1}) h(0, t^*_K) v(0, t^*_K) W_i(X(t^{n+1}; 0, t^*_K), t^{n+1}) \Bigg\} \qquad (19)$$

The procedure followed is to select the integration points t^*_k, determine the integration weights given in (19), forward

track from the boundary from t_k^* to t^{n+1} to determine $\hat{X}$, and finally to calculate $W_i(\hat{X}, t^{n+1})$ for each i. The tracking scheme is described by (11), with $x_p(t_k^*)$ representing the location of the boundary. Equation (13) is again used to calculate $W_i(\hat{X}, t^{n+1})$.

Selection of the appropriate number of time integration points is dependent on two requirements: accurate integration of the integral in (18) when $W \equiv 1$ to obtain the correct total mass, and proper distribution of the tracked mass from the boundary into the spatial grid. The implications of the first requirement are related to the behavior of v and h between t^n and t^{n+1}. If the customary assumption of linearity for both variables is made, then all terms on the right-hand side of (19) reduce to a function of v and h at t^n and t^{n+1}. So, in effect, no intermediate integration points are needed. Although this assumption will undoubtedly be used in most applications, it is not necessary for this method.

The second requirement will usually be more restrictive than the first. Improper distribution of mass leads to failure to conserve mass locally on $[x_{i-(1/2)}, x_{i+(1/2)}]$ and is manifested by concentrations near the boundary which are not equal to h, when h is constant in time and t approaches infinity. These concentrations may be slightly less than or greater than h and can produce slight oscillations near sharp concentration fronts. To aid in properly distributing mass, we have incorporated strategic time integration points (STIP) into the method. The STIPs are determined as were the SSIPs, by backtracking from the points on the spatial grid where there is a change in slope of the test function. If the backtracking encounters the inflow boundary, then the time at which the boundary is encountered becomes a STIP. An important component of our method is, therefore, to backtrack at the start of each time step from the three points in each spatial grid cell where the slope of the test function changes. Those tracked locations that intersect a boundary become STIPs, while those locations that remain on the spatial grid become SSIPs. The range of integration points given in (16) can now be reduced by substituting the largest STIP that is less than $t_{i+(1/2)}^*$ for t^n (assuming $t_{i+(1/2)}^* > t^n$) and substituting the smallest STIP that is greater than $t_{i-(1/2)}^*$ for t^{n+1} (assuming $t_{i-(1/2)}^* < t^{n+1}$) as $W_i(\hat{X}, t^{n+1})$ is zero for t^* outside of this range.

For constant-coefficient problems, there is no need for any additional time integration points other than the STIPs. Use of only the STIPs will properly distribute the inflowing mass. For variable-coefficient problems, it is sometimes necessary to add additional time integration points to insure proper distribution. Additional integration points may be added at uniform intervals between $t_{i+(1/2)}^*$ and $t_{i-(1/2)}^*$. The addition of NS new time integration points between $t_{i-(1/2)}^*$ and $t_{i+(1/2)}^*$ is sufficient to impart the same resolution to the boundary flux tracking that is contained in the tracking of spatial integration points. For most problems, fewer than NS such new points per interval are required to insure proper mass distribution.

Application of boundary conditions to a body-centered grid requires some discussion. Referring to Figure 6, location $x_{1/2}$ corresponds to $x = 0$ in the previous discussion, and $h(0, t)$ is really $h(x_{1/2}, t)$. When the Dirichlet condition is employed, consideration must be given as to how $c(x, t^n)$ is defined when $x_{1/2} \le x \le x_1$. These values are required for the numerical evaluation of the integral in (10). Linear interpolation between $x_{1/2}$ and x_1 is used to determine these values.

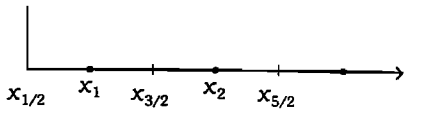

Fig. 6. Body-centered finite-difference grid showing boundary location.

Neumann condition. The boundary flux integral for the Neumann condition becomes

$$-\left(\int_{t^n}^{t^{n+1}} c(0, t)v(0, t)W_i(\hat{X}, t^{n+1})\, dt - \int_{t^n}^{t^{n+1}} h(0, t)W_i(\hat{X}, t^{n+1})\, dt\right) \tag{20}$$

The specified flux occurs at $x_{1/2}$ and the boundary condition can be stated as

$$-D\frac{\partial c}{\partial x}(x_{1/2}, t) = h(0, t) \tag{21}$$

Approximating $\partial c/\partial x$ by

$$\frac{c(x_1, t) - c(x_{1/2}, t)}{x_1 - x_{1/2}},$$

(21) can be rearranged to solve for $c(x_{1/2}, t)$:

$$c(x_{1/2}, t) = c(x_1, t) + \frac{h(0, t)}{D}(x_1 - x_{1/2}) \tag{22}$$

Then, as in the Dirichlet condition, linear interpolation defines $c(x, t^{n+1})$ for $x_{1/2} \le x \le x_1$. The advective integral is treated as described in the previous section.

Total-flux condition. The boundary integral in (14) actually represents the total solute flux through the boundary. The boundary integral for the total-flux boundary is

$$-\int_{t^n}^{t^{n+1}} h(0, t)W_i(\hat{X}, t^{n+1})\, dt$$

and the boundary condition is

$$v(x_{1/2}, t)c(x_{1/2}, t) - D\frac{\partial c}{\partial x}(x_{1/2}, t) = h(0, t) \tag{23}$$

Again approximating $\partial c(x_{1/2}, t)/\partial x$ by

$$\frac{c(x_1, t) - c(x_{1/2}, t)}{x_1 - x_{1/2}}$$

gives the following value for $c(x_{1/2}, t)$:

$$c(x_{1/2}, t) = \frac{c(x_1, t) + [h(0, t)(x_1 - x_{1/2})]D^{-1}}{1 + [v(x_{1/2}, t)(x_1 - x_{1/2})]D^{-1}} \tag{24}$$

Using this value, the dispersive flux across the boundary can be calculated from the advective flux. The advective flux can then be treated as previously described.

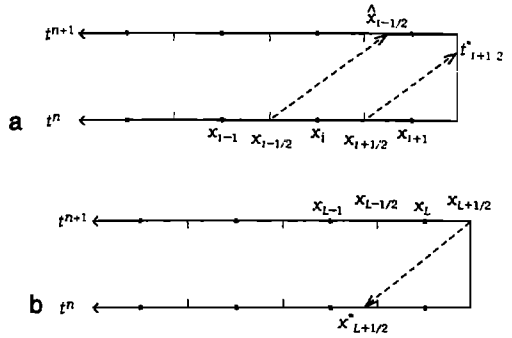

Fig. 7. (*a*) Characteristic line intersecting outflow boundary when forward tracking from time level n. (*b*) Backtracking from boundary to determine $x^*_{L+(1/2)}$.

Outflow Boundaries

Outflow boundaries come into play when forward tracking from $x_{i+(1/2)}$ at t^n results in the case that the boundary (assumed to be at $x = l$) is intersected at $t^*_{i+(1/2)} < t^{n+1}$ (Figure 7). To obtain a modified version of (7) for this case, we consider Figure 7*b*. Note that the equation for the last finite volume $[x_{L-(1/2)}, x_{L+(1/2)}]$, where L denotes the finite-difference cell adjacent to the outflow boundary, does not cover the triangular space-time region with corners (l, t^{n+1}), (l, t^n), and $(x^*_{L+(1/2)}, t^n)$. We seek an equation corresponding to this region, requiring us to designate an associated unknown. We let $W_{L+1}(x, t)$ be the test function.

Before developing the outflow equation, we must determine the form of W_{L+1}. The point $x^*_{L+(1/2)}$ is an SSIP. According to our scheme, those spatial integration points between $x^*_{L-(1/2)}$ and $x^*_{L+(1/2)}$ send all of their mass to the interior of the grid, while those between $x^*_{L+(1/2)}$ and l send all of their mass to the boundary. The mass associated with $x^*_{L+(1/2)}$ at t^n is split between the interior and the boundary according to the proportions of mass lying to the left and right of $x^*_{L+(1/2)}$. With this understanding, we can define the discontinuous function $W_{L+1}(x, t)$ as

$$W_{L+1}(x, t^{n+1}) = 0 \qquad 0 \le x < l$$

$$W_{L+1}(l, t) = 1 \qquad t^n \le t \le t^{n+1}$$

and correspondingly:

$$W_L(x, t^{n+1}) = 1 \qquad x_{L-(1/2)} + \overline{\Delta x}_L \le x \le l$$

$$W_L(l, t) = 0 \qquad t^n \le t < t^{n+1}$$

These definitions allow us to separate the outflow boundary terms from the conservation equation (7) for interior cells. In particular, (7) may be written for $i = L$ by simply changing the limits in the right-hand side integral of (9) to zero to $x^*_{L+(1/2)}$.

The outflow equation can now be derived. All three types of boundary conditions that were discussed for inflow boundaries are applicable to outflow boundaries. However, in practice the Neumann condition with no dispersive outflow is used almost exclusively in groundwater solute transport problems. Therefore this is the only condition that is discussed here. Details on the other boundary types are provided elsewhere (T. F. Russell and R. W. Healy, manuscript in preparation, 1993). It is convenient to refer to (14), since it exemplifies some of the necessary modifications to (7). The first term in (7) or (14) does not appear because the triangular region of interest does not meet the spatial domain at t^{n+1}. Essentially the mass that was represented by this integral is now represented by the advective component of the boundary flux integral. The dispersion term corresponding to $(x_{i-(1/2)}, t^{n+1})$ in (14) is now evaluated at (l, t^{n+1}) with time weight Δt, while the term corresponding to $(x_{i+(1/2)}, t^{n+1})$ now has a time weight of zero and therefore does not appear. The limits on the first integral on the right-hand side of (7) are adjusted accordingly, and the second integral on that side is transformed to an integral over time by replacing dx with $v(l, t)\,dt$. Combining these observations and noting that $W_{L+1} \equiv 1$ for all terms, we can write

$$\int_{t^n}^{t^{n+1}} \left[v(l, t)c(l, t) - D\frac{\partial c}{\partial x}(l, t) \right] dt + D\Delta t \frac{\partial c}{\partial x}(l, t^{n+1})$$

$$= \int_{x^*_{L+(1/2)}}^{l} c(x, t^n)\,dx + \int_{t^n}^{t^{n+1}} f(l, t)(t - t^n)v(l, t)\,dt \tag{25}$$

Imposing the Neumann condition with zero dispersive flux,

$$\int_{t^n}^{t^{n+1}} v(l, t)c(l, t)\,dt = \int_{x^*_{L+(1/2)}}^{l} c(x, t^n)\,dx + \int_{t^n}^{t^{n+1}} f(l, t) \cdot (t - t^n)v(l, t)\,dt \tag{26}$$

Equation (26) is solved for $c^{n+1}_{L+(1/2)} = c(l, t^{n+1})$. In so doing, it is assumed that $c(l, t)$ varies linearly in time for $t^n \le t \le t^{n+1}$ and that $c(x, t^{n+1})$ varies linearly in space for $x_L \le x \le x_{L+(1/2)} = l$. The trapezoid rule is used for the boundary flux integral. With intermediate temporal integration points, t^*_k, defined by (16), we follow (17), (18), and (19) to get

$$\int_{t^n}^{t^{n+1}} v(l, t)c(l, t)W_{L+1}(l, t)\,dt$$

$$= \frac{1}{2}\left\{ \sum_{k=1}^{K-1} (t^*_{k+1} - t^*_{k-1})v(l, t^*_k)c(l, t^*_k) + (t^*_1 - t^*_0)v(l, t^*_0)c(l, t^*_0) + (t^*_K - t^*_{K-1})v(l, t^*_K)c(l, t^*_K) \right\} \tag{27}$$

where $t^*_0 = t^n$, $t^*_K = t^{n+1}$, and $K + 1$ is the total number of integration points used and is equal to the number of spatial integration points that lie in $[x^*_{L+(1/2)}, l]$ at t^n. Each t^*_k corresponds to the time at which a spatial integration point within that interval intersects the boundary at l when forward tracking from t^n. The first integral in the right-hand side of (26) is evaluated as previously described, keeping in mind that the integration point $x^*_{L+(1/2)}$ now carries only the mass located to its right as shown in Figure 7*b*. The integral containing f is evaluated in analogy to (27).

Previous papers about the finite-element ELLAM formulation [*Celia et al.*, 1990; *Russell*, 1990] have considered

TABLE 1. Mean-Square Errors Between Calculated and Analytical Results for Test Problem 1

	Cr					
	0.0125	0.125	0.333	0.700	1.00	2.50
			Pe = 0.2			
FVE2	4.4E−5*	2.4E−6	3.0E−7	1.1E−6	4.7E−7	2.6E−6
FVE4	1.1E−6	2.3E−7	1.4E−8	1.8E−7	4.7E−7	2.6E−6
FVE8	2.5E−7	6.4E−9	3.5E−8	2.1E−7	4.7E−7	2.6E−6
FVE16	5.2E−8	6.4E−9	4.6E−8	2.3E−7	4.7E−7	2.6E−6
FVEE	1.0E−9	6.4E−9	5.1E−8	2.3E−7	4.7E−7	2.6E−6
CD	1.3E−8	1.3E−8	1.7E−8	4.3E−8	9.8E−8	2.0E−6
BD	1.8E−5	2.3E−5	3.3E−5	5.6E−5	7.9E−5	2.5E−4
			Pe = 2.			
FVE2	1.3E−4	7.8E−5	1.7E−5	2.2E−5	7.7E−8	5.7E−7
FVE4	3.4E−5	9.9E−6	1.1E−6	7.9E−8	7.7E−8	5.7E−7
FVE8	8.3E−6	1.7E−7	1.2E−7	2.3E−8	7.7E−8	5.7E−7
FVE16	1.9E−6	1.7E−7	5.8E−8	3.5E−8	7.7E−8	5.7E−7
FVEE	1.9E−7	1.7E−7	5.9E−8	4.0E−8	7.7E−8	5.7E−7
CD	3.0E−6	3.0E−6	3.4E−6	5.1E−6	8.2E−6	8.7E−5
BD	4.4E−4	5.2E−4	6.8E−4	1.0E−3	1.3E−3	2.7E−3
			Pe = 20			
FVE2	1.3E−3	9.6E−4	3.3E−4	1.1E−4	9.2E−9	1.0E−7
FVE4	5.3E−4	2.2E−4	5.2E−5	1.1E−5	9.2E−9	1.0E−7
FVE8	2.0E−4	5.2E−5	2.4E−5	6.7E−6	9.2E−9	1.0E−7
FVE16	8.6E−5	5.2E−5	2.1E−5	5.8E−6	9.2E−9	1.0E−7
FVEE	6.2E−5	5.2E−5	2.1E−5	5.7E−5	9.2E−9	1.0E−7
CD	5.6E−4	5.7E−4	6.0E−4	7.2E−4	8.9E−4	2.5E−3
BD	2.9E−3	3.2E−3	3.8E−3	4.8E−3	5.5E−3	8.7E−3

Cr is Courant number. *Pe* is cell Peclet number. FVEX is FVELLAM with NS = *X*. FVEE is FVELLAM with exact integration. CD is centered finite-difference method. BD is backward finite-difference method.

*Read 4.4E−5 as 4.4×10^{-5}.

temporal discretizations of the outflow boundary, in which the triangular space-time region discussed above is subdivided into elements corresponding to a series $c(l, t_1^*), \cdots, c(l, t_K^*) = c(l, t^{n+1})$ of unknowns. The idea is that the temporal resolution of the outward flux reflects the same level of detail as the spatial resolution of the concentration profile approaching the boundary. This could be done with FVELLAM as well and is addressed elsewhere (T. F. Russell and R. W. Healy, manuscript in preparation, 1993).

Mass Conservation

Equation (7), in conjunction with appropriate boundary conditions selected from (17), (20), (23), and (25), and the discretizations of each of these equations represent a conservative statement of solute transport for each time step over the entire domain $x \in [0, l]$. This is easily seen by noting that the test functions (and approximate test functions) sum exactly to 1 over all interior cells and inflow and outflow boundaries. Care must be taken, however, in evaluating the terms in those equations to insure mass conservation in practice. The mass at the beginning of each time step $[t^n, t^{n+1}]$ must be integrated correctly, motivating the forward tracking scheme we have employed. Also, boundary fluxes must be integrated correctly; as with any scheme, FVELLAM can conserve mass only to the accuracy of its boundary fluxes.

RESULTS

Problem 1

In the first test problem, solute transport through a one-dimensional vertical column was simulated for a period of 2 hours. A steady flow of water was maintained in the column. Initially, the water in the column was solute free. At time 0, the concentration of inflowing water was set to c_0. *Ogata and Banks* [1961] give the analytical solution to this problem. The simulation was begun at time 1 hour, with initial concentrations in the column determined by the analytical solution at that time. This was done to avoid oscillation at early times due to the incompatibility of initial and boundary conditions. Simulations were run with the finite volume ELLAM code and with a standard finite-difference code [*Healy*, 1990] using centered (CD) and backward (BD) differencing for spatial and temporal derivatives. The following constants were used:

$$\Delta x = 2 \text{ cm} \qquad v = 25 \text{ cm/h}$$

$$D = \alpha v \qquad \alpha = 0.1,\ 1.0,\ 10.0 \text{ cm}$$

$$\Delta t = 0.001,\ 0.01,\ 0.026667,\ 0.056,\ 0.08,\ 0.20$$

$$\text{NS} = 2,\ 4,\ 8,\ 16$$

Values for α, Δt, and NS were held constant within each simulation. The values of α correspond to cell Peclet numbers (*Pe*) of 20, 2, and 0.2, respectively, while the time step sizes correspond to Courant numbers (*Cr*) of 0.0125, 0.125, 0.333, 0.7, 1.0, and 2.5.

Results, in terms of mean-square errors, are shown in Table 1. Included in that table are results from using exact integration of the storage integral in (9) with FVELLAM. These values, in theory, represent the most accurate results that can be obtained by the method. Comparison of these values with other FVELLAM results gives an indication of

the improvement in accuracy obtained as NS is increased. For Pe equal to 2 and 20, FVELLAM clearly outperforms the standard FDMs, especially for the higher values of Cr. Figure 8 shows a comparison of results of the different methods for $Pe = 20$ and $Cr = 0.7$. Large numerical oscillations are present in the CD results, while numerical dispersion dominates the BD results. There is little visual difference among the FVELLAM results, with the exception of those for NS = 2, which display a slight amount of numerical dispersion. At $Pe = 0.2$, the FVELLAM results have an accuracy similar to that produced by the CD method. While the FVELLAM approach may offer no advantage for this type of dispersion-dominated problem for which standard numerical methods work well, it is noteworthy that the FVELLAM approach can produce good results at low Courant numbers. These types of problems have typically been very difficult to solve accurately by characteristic methods without added numerical dispersion [*Neuman*, 1981; *Healy and Russell*, 1989]. Whereas CD and BD show decreasing accuracy with increasing Cr at any value of Pe, the trend in accuracy of FVELLAM is more complex. There appears to be an optimum value of Cr that produces the best results. That value increases as Pe increases, being about 0.333 for $Pe = 0.2$, 0.7 for $Pe = 2.0$, and 1.0 for $Pe = 20.0$. For values of Cr that are less than this optimum value, slight amounts of numerical dispersion may creep into the calculations because the number of numerical integrations (and interpolations) increases with an increasing number of time steps. At values of Cr greater than the optimum value, the reduced accuracy is probably due to time truncation error from the use of backward differencing in (4). For all values of NS, the amount of numerical dispersion tends to increase as Cr decreases and as Pe increases. The improvement in results gained by increasing NS appears to be inversely related to Cr, with the most improvement occurring at $Cr = 0.0125$. For all runs listed in Table 1 (and all other tables), mass was conserved to machine accuracy (approximately 7 digits).

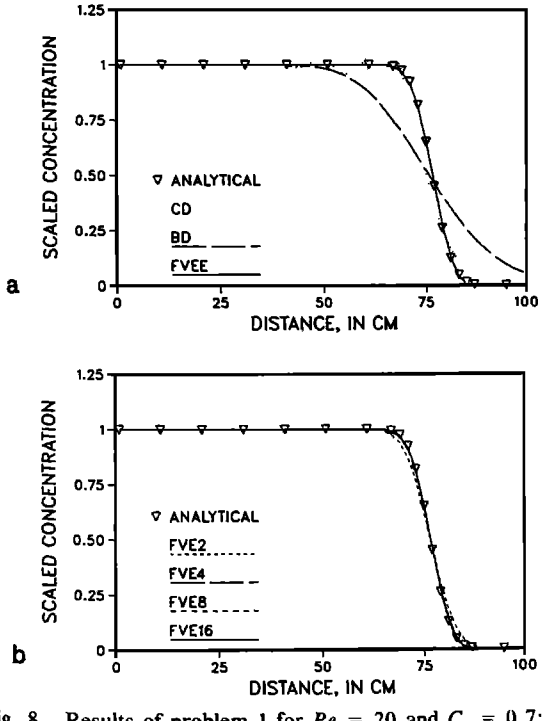

Fig. 8. Results of problem 1 for $Pe = 20$ and $C_r = 0.7$: (*a*) centered finite-difference method (CD), backward finite-difference method (BD), and FVELLAM with exact integration (FVEE); (*b*) FVELLAM with NS = 2, 4, 8, and 16.

TABLE 2. Mean-Square Errors Between Calculated and Analytical Results for Variable Grid Spacing Version of Test Problem 1 for Different Values of Time Step (Δt) and Dispersivity (α)

	Δt			
	0.001	0.01	0.056	0.08
		$\alpha = 10$		
FVE2	8.97E−6*	6.13E−6	1.94E−7	3.35E−7
FVE4	2.25E−6	9.29E−7	2.84E−7	6.33E−7
FVE8	5.47E−7	4.25E−8	3.36E−7	7.51E−7
FVE16	1.31E−7	1.12E−8	3.63E−7	7.84E−7
FVEE	1.44E−8	1.76E−8	3.76E−7	7.95E−7
CD	1.11E−7	1.13E−7	1.84E−7	2.87E−7
		$\alpha = 1.0$		
FVE2	2.20E−4	1.63E−4	1.39E−6	6.55E−6
FVE4	6.43E−5	3.14E−5	2.65E−7	3.57E−7
FVE8	1.71E−5	2.69E−6	1.34E−7	4.07E−7
FVE16	4.45E−6	8.25E−7	1.51E−7	5.20E−7
FVEE	7.63E−7	7.06E−7	1.76E−7	5.67E−7
CD	1.75E−5	1.77E−5	2.24E−5	2.86E−5
		$\alpha = 0.1$		
FVE2	1.54E−3	1.29E−3	1.84E−4	1.68E−4
FVE4	7.27E−4	4.71E−4	4.09E−5	3.98E−5
FVE8	3.47E−4	1.97E−4	2.85E−5	3.37E−5
FVE16	2.29E−4	1.99E−4	2.77E−5	3.45E−5
FVEE	2.57E−4	2.13E−4	2.91E−5	3.50E−5
CD	1.24E−3	1.24E−3	1.33E−3	1.43E−3

*Read 8.97E−6 as 8.97×10^{-6}.

To further examine the sensitivity of results to NS, we look at a variable-coefficient case that is produced when the grid spacing is nonuniform. Table 2 shows results obtained with the following modifications to test problem 1:

$$\Delta x_1 = 0.1$$

$$\Delta x_j = 1.2\Delta x_{j-1} \qquad j = 2, \cdots, 19$$

$$\Delta x_j = 3 \qquad j > 19$$

$$\Delta t = 0.001,\ 0.01,\ 0.056,\ 0.08$$

For this version of the problem the simulation ran from an initial time of 0.3 hours up to 2.3 hours in order to assure that the solute front remained within the variably spaced section of the grid. In Table 2 the same trends are present that were in Table 1. It does appear that the FVELLAM results are slightly more sensitive to the value of NS for variable spacing than for uniform spacing.

Problem 2

The second test problem involves fluid injection at a constant rate from a fully penetrating well in a confined aquifer. Axial symmetry is assumed, and radial coordinates are used in the simulation. The solute concentration within the aquifer is initially 0, and the concentration of the injected water is c_0. Analytical solutions to this problem have been developed by *Tang and Babu* [1979] and *Hsieh* [1986]. *Hoopes and Harleman* [1967] and *Gelhar and Collins* [1971]

TABLE 3. Mean-Square Errors Between Calculated and Analytical Results for Test Problem 2

	Δt			
	0.5	5.	50.	250.
		$\alpha = 10.$		
FVE2	9.54E−5*	6.80E−5	2.01E−6	1.14E−5
FVE4	2.35E−5	1.02E−5	5.42E−7	1.13E−5
FVE8	5.29E−6	5.52E−7	4.68E−7	1.12E−5
FVE16	1.01E−6	1.27E−8	4.79E−7	1.12E−5
FVEE	7.94E−8	3.96E−8	4.85E−7	1.12E−5
CD	7.36E−6	7.37E−6	9.84E−6	2.80E−4
		$\alpha = 2$		
FVE2	1.73E−3	1.26E−3	3.14E−5	8.71E−6
FVE4	4.77E−4	2.14E−4	4.08E−6	8.65E−6
FVE8	1.14E−4	1.50E−5	5.15E−6	9.08E−6
FVE16	2.46E−5	6.63E−6	5.70E−6	9.19E−6
FVEE	9.26E−6	8.40E−6	5.87E−6	9.34E−6
CD	7.04E−5	7.10E−5	1.62E−4	7.16E−3

*Read 9.45E−5 as 9.45×10^{-5}.

developed approximate analytical solutions. The aquifer was assumed to be 10 m thick. Spacing in the radial direction increased from 0.1 m at the injection well by a factor of 1.2 until a maximum size of 5 m was reached. The length of the grid in the radial direction was 847 m. Injection rate was 225 m^3/h, and the radial flow boundary was set at a constant pressure head. A pumping period of 2000 hours was simulated. The following parameter values were used:

$$D = \alpha v \qquad \alpha = 2., 10. \quad \text{m}$$

$$\Delta t = 0.5, 5., 50., 250. \quad \text{hours}$$

$$\text{NS} = 2, 4, 8, 16$$

Table 3 shows results in terms of mean-square error between calculated and analytical [*Hsieh*, 1986] results at 2000 hours for FVELLAM and CD. Figure 9 shows a comparison of results at 500, 1000, and 2000 hours for Δt = 50 and $\alpha = 2$. At time 2000, the accuracy of the CD results generally lies between that of FVE4 and FVE8 for time step sizes less than 50 hours. At a time step size of 250 hours, all FVELLAM results are much more accurate than the CD results. Numerical dispersion affects the FVELLAM results for low values of NS. This is manifested by the smearing of the solute front. Numerical dispersion increases as the time step size and the value of α decrease.

DISCUSSION

The finite-volume Eulerian-Lagrangian localized adjoint method represents a significant step in the implementation of ELLAM theory. By application of an integrated finite-difference approach, we believe that we have created a framework from which multiple-dimension transport simulators can be developed. Our method conserves mass both globally and locally on Lagrangian space-time elements, is capable of treating general boundary conditions in a consistent and straightforward fashion, and is not limited by restrictions on the Courant number. Except for boundary contributions, the matrix equation that is produced by FVELLAM is symmetric, and therefore generalized methods of preconditioned conjugate gradients may be used to solve the equation for multidimensional problems. We have demonstrated that FVELLAM can produce accurate results for all test problems examined here. The method is particularly well suited to solve advection-dominated problems that are difficult to solve by standard methods.

Although FVELLAM requires more computational effort than does the standard finite-difference method for a problem with the same spatial and temporal discretization, FVELLAM permits the use of coarser grids and larger time steps with little loss of accuracy. Therefore a large savings in computational effort can be realized. For any fixed spatial grid, the amount of additional computation time required by FVELLAM relative to standard FDM is related to the number of integration points used in each cell (NS) and the Courant number. The most time-consuming aspect of FVELLAM is tracking, and the amount of tracking increases as NS increases. Also, because this code tracks on a cell-by-cell basis, the work required increases as the Courant number increases because the number of cells that each point passes through increases. It should be noted that the amount of work required by FVELLAM is independent of the cell Peclet number. It is not practical to develop a formula to predict the amount of work required by FVELLAM, but we can compare work among methods used in test problem 1. Table 4 shows time required, per time step, to solve the ADE for test problem 1 for a uniform grid (Δx = 2) of 150 nodes. Linking Tables 1 and 4 gives an idea of the relative work required by each method to solve to a given level of accuracy. For example, at $Pe = 2.0$, NS = 2, and Cr = 2.50 FVELLAM produces a mean-square error of 0.566 $\times 10^{-6}$ in 5.61 s of CPU time, while for centered differencing the best accuracy (0.299×10^{-5}) is obtained for Cr = 0.0125 and requires 44.80 s. So, FVELLAM produces more

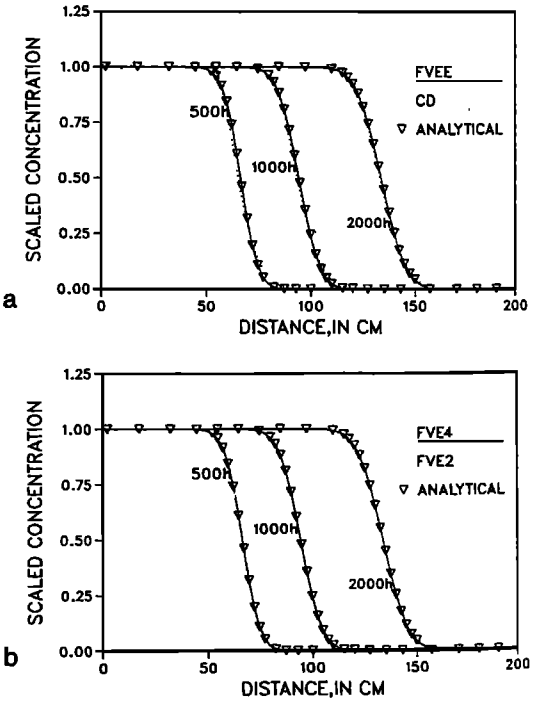

Fig. 9. Results of problem 2 for $\alpha = 2$ and $\Delta t = 50$: (*a*) FVELLAM with exact integration (FVEE) and centered finite-difference method (CD); (*b*) FVELLAM with NS = 2 and 4.

accurate results in less computation time than the FDM for this example.

In viewing Table 4, it should be kept in mind that these times are only for solving the ADE. Most problems of practical concern involve solving the groundwater flow equation in addition to the ADE. For these problems, the relative differences in total computation time per time step among the different methods will be much less than that shown in Table 4. Also when treating two- or three-dimensional problems, solving the matrix equation requires a larger proportion of computational time than for one-dimensional problems; therefore the tracking procedure at higher dimensions will be less of a consideration.

For many problems, the work requirements of FVELLAM could be reduced dramatically by incorporation of an adaptive scheme to automatically determine the number of spatial integration points required for each cell (as opposed to using a fixed number for each cell). With this approach, NS could be given values of, for example, 8 or 16 in cells that lie on a sharp concentration front. Cells that lie in regions where there was little change in concentration would require an NS value of only 2. Such an adaptive scheme will be a necessary component of any practical multidimensional FVELLAM.

There are a few limitations to our method that should be addressed. For problems with a high Peclet number and a low Courant number, numerical dispersion can enter into the solution if NS is not great enough (Table 1). It is doubtful whether the adaptive selection of NS as described above would alleviate this problem. These problems will be more easily solved with FVELLAM if the grid spacing is decreased (resulting in a decrease in Pe) or the time step size is increased (resulting in an increase in Cr).

Slight oscillations can appear in results of problems involving steep concentration fronts, if there are not a sufficient number of finite-difference nodes across the front. *Russell* [1985] found that with MMOC three to four nodes were needed across the width of the front to avoid oscillations. The width of the front was assumed to be the distance between the points where concentrations were equal to 0.05 and 0.95 of the difference in concentration between the head and the toe of the front. We have found FVELLAM to behave similarly to MMOC in this respect. The number of nodes required across a front is therefore independent of the steepness of the front. This requirement is much less stringent than the node-spacing requirement for the FDM in order to avoid numerical dispersion or oscillation, $Pe \leq 2$, which forces the number of nodes across a front to increase as the dominance of advection increases. This can be qualitatively demonstrated by considering the analytical solution to problem 1. The cell Peclet number is inversely proportional to α. So a decrease by a factor of 100 in α would require Δx to also be reduced by a factor of 100 to maintain $Pe = 2$. However, according to the analytical solution for problem 1, the width of the solute front increases proportional to $\alpha^{1/2}$. So a hundredfold decrease in α would require that Δx be reduced by only a factor of 10 to avoid oscillations with FVELLAM. Note that this would multiply Pe by 10: that is, as α decreases we can decrease Δx as $\alpha^{1/2}$, thereby increasing Pe as $\alpha^{-1/2}$. For example, for the case $Pe = 20$ in problem 1, we have run tests in which we decrease α and Δx by factors of 100 and 10, respectively, resulting in the value $Pe = 200$. Test results exhibited essentially the same behavior as those reported in Table 1. Thus FVELLAM behavior depends on the relationship between the front width and the grid size, as one would desire, rather than on the Peclet number.

TABLE 4. Work Required, in Seconds, to Solve the Advection Dispersion Equation for an Individual Time Step in Test Problem 1

	Courant Number				
	0.0125	0.125	0.7	1.	2.5
FVE2	0.327	0.375	0.426	0.446	0.561
FVE4	0.367	0.420	0.447	0.503	0.640
FVE8	0.436	0.511	0.553	0.612	0.792
FVE16	0.581	0.684	0.765	0.840	1.137
CD	0.224	0.255	0.255	0.276	0.276

As presented here, FVELLAM is used only for one-dimensional applications. Extension of the method to multiple dimensions is currently in development. While conceptually straightforward, efficient implementation of this extension faces several challenges. Local mass conservation will be more difficult to achieve with the forward tracking scheme because of the multidimensional velocity field. An increased number of SSIPs will be required (at least nine for each finite-difference cell in two dimensions) and will result in increased computer storage and execution time. The use of a backtracking scheme to evaluate the integral in (9) may be an attractive alternative in areas of smoothly varying concentration. This raises the possibility of adaptively selecting, on a cell-by-cell basis, either the forward or backtracking schemes to evaluate the integral. Another concern in multiple dimensions is treatment of boundary fluxes. The integrals that represent these fluxes will need to be evaluated over both space and time.

SUMMARY

A new method has been developed and tested for solving the one-dimensional advection-dispersion equation. The finite-volume Eulerian-Lagrangian localized adjoint method has been demonstrated to accurately and efficiently solve problems that are strongly advection dominated. For dispersion-dominated problems, the new method compares well in terms of accuracy with the standard centered finite-difference method, but is slightly less efficient than the latter method in terms of computation time. The method is mass conservative and is not restricted by limitations on the size of the Courant number.

The FVELLAM approach extends previous ELLAM results by application of an integrated finite-difference approximation scheme and by its ability to conserve mass locally on each finite volume. Mass conservation is facilitated by application of a numerical integration scheme at the current time level followed by forward tracking of quadrature points to the next time level. Forward tracking also eliminates the difficulty of intercepting inflow boundaries that is encountered when backtracking is used (as is common in most characteristic methods). Problems with variable coefficients can be treated in either Cartesian or radial coordinates. Detailed information was presented on treatment of integration, tracking, and boundary algorithms.

APPENDIX: RADIAL COORDINATES

Equation (7) can be written in radial coordinates simply by replacing x with r and multiplying each term by $2\pi r$. The mass storage term on the left-hand side of the equation becomes

$$\int_{r_{i-(1/2)}}^{r_{i+(1/2)}} 2\pi r c(r, t^{n+1})\, dr$$

Once again assuming a linear change in concentration between adjacent nodes and applying a weighted trapezoid rule produces the following approximation (exact for linear c) which is analogous to (8) for interior cells:

$$\begin{aligned}
&\int_{r_{i-(1/2)}}^{r_{i+(1/2)}} 2\pi r c(r, t^{n+1})\, dr \\
&= 2\pi\Delta r_i\left\{\frac{1}{4}\frac{\Delta r_i}{\Delta r_i+\Delta r_{i-1}} r_{i-(1/3)} c(r_{i-1}, t^{n+1})\right. \\
&\quad + \left(\frac{r_i}{2}+\frac{1}{4}\left[\frac{\Delta r_{i-1}}{\Delta r_i+\Delta r_{i-1}} r_{i-(1/3)}\right.\right. \\
&\quad \left.\left. + \frac{\Delta r_{i+1}}{\Delta r_i+\Delta r_{i+1}} r_{i+(1/3)}\right]\right) c(r_i, t^{n+1}) \\
&\quad \left. + \frac{1}{4}\frac{\Delta r_i}{\Delta r_i+\Delta r_{i+1}} r_{i+(1/3)} c(r_{i+1}, t^{n+1})\right\},
\end{aligned} \tag{A1}$$

where

$$r_{i-(1/3)} = \tfrac{5}{6} r_{i-(1/2)} + \tfrac{1}{6} r_{i+(1/2)},$$

$$r_{i+(1/3)} = \tfrac{1}{6} r_{i-(1/2)} + \tfrac{5}{6} r_{i+(1/2)}.$$

The mass storage term for time level n, which is given by an analogue of (9), can be written for the specific case of zero Courant number as

$$\begin{aligned}
&\int_{r^*_{i-(1/2)}}^{r^*_{i+(1/2)}} 2\pi r c(r, t^n)\, dr \\
&= \int_0^l 2\pi r c(r, t^n) W_i(r, t^n)\, dr \\
&\equiv 2\pi\left\{\sum_{j=1}^{NS-1} c\left(r_{i-(1/2)}+\frac{j\Delta r_i}{NS}, t^n\right)\frac{\Delta r_i}{NS}\left(r_{i-(1/2)}+\frac{j\Delta r_i}{NS}\right)\right. \\
&\quad + \frac{1}{2} c(r_{i-(1/2)}, t^n) W_i(r_{i-(1/2)}, t^{n+1}) \\
&\quad \cdot\left[\left(r_{i-(1/2)}-\frac{\Delta r_{i-1}}{3NS}\right)\frac{\Delta r_{i-1}}{NS} + \left(r_{i-(1/2)}+\frac{\Delta r_i}{3NS}\right)\frac{\Delta r_i}{NS}\right] \\
&\quad + \frac{1}{2} c(r_{i+(1/2)}, t^n) W_i(r_{i+(1/2)}, t^{n+1}) \\
&\quad \cdot\left[\left(r_{i+(1/2)}-\frac{\Delta r_i}{3NS}\right)\frac{\Delta r_i}{NS}\right. \\
&\quad \left.\left. + \left(r_{i+(1/2)}+\frac{\Delta r_{i+1}}{3NS}\right)\frac{\Delta r_{i+1}}{NS}\right]\right\}
\end{aligned} \tag{A2}$$

We wish to ensure that the coefficients for c_{i-1}, c_i, and c_{i+1} in (A1) are identical to those in (A2). We look at just the coefficient for c_{i-1}. The contribution from c_{i-1} that appears in (A2) can be written

$$\begin{aligned}
&2\pi\frac{\Delta r_i}{\Delta r_i+\Delta r_{i-1}}\left\{W_i(r_{i-(1/2)}, t^{n+1})\right. \\
&\quad \cdot\left[\left(r_{i-(1/2)}+\frac{\Delta r_i}{3NS}\right)\frac{\Delta r_i}{2NS} + \left(r_{i-(1/2)}-\frac{\Delta r_{i-1}}{3NS}\right)\frac{\Delta r_{i-1}}{2NS}\right] \\
&\quad \left. + \frac{\Delta r_i}{NS}\sum_{j=1}^{(NS/2)-1}\left(1-\frac{2j}{NS}\right)\left(r_{i-(1/2)}+j\frac{\Delta r_i}{NS}\right)\right\}
\end{aligned}$$

Equating this term with the corresponding coefficient in (A1) and simplifying produces the following formula for $W_i(r_{i-(1/2)}, t^{n+1})$:

$$\begin{aligned}
W_i(r_{i-(1/2)}, t^{n+1}) = \Delta r_i\left(r_{i-(1/2)}+\frac{\Delta r_i}{3NS}\right)\left[\Delta r_{i-1}\left(r_{i-(1/2)}\right.\right. \\
\left.\left. -\frac{\Delta r_{i-1}}{3NS}\right) + \Delta r_i\left(r_{i-(1/2)}+\frac{\Delta r_i}{3NS}\right)\right]^{-1}
\end{aligned} \tag{A3}$$

When uniform spacing is used, this equation simplifies to

$$W_i(r_{i-(1/2)}, t^{n+1}) = \frac{1}{2} + \frac{\Delta r}{6NS r_{i-(1/2)}} \tag{A4}$$

The value of $W_i(r_{i+(1/2)}, t^{n+1})$ can then be obtained as

$$W_i(r_{i+(1/2)}, t^{n+1}) = 1 - W_{i+1}(r_{i+(1/2)}, t^{n+1}) \tag{A5}$$

As with Cartesian coordinates, $W_i(r, t^{n+1}) = 1$ when $r_{i-(1/2)} + (\Delta r_i/NS) \le r \le r_{i+(1/2)} - (\Delta r_i/NS)$. Linear interpolation is used when r falls outside that interval. Equation (13) may be used to determine $W_i(\hat{r}, t^{n+1})$ for radial coordinates by simply replacing the term $\Delta x_i/(\Delta x_i + \Delta x_{i-1})$ with the right-hand side of (A3) and the term $\Delta x_i/(\Delta x_i + \Delta x_{i+1})$ with the right-hand side of (A5).

With W_i as defined above, it can be shown that

$$\int_0^l W_i(r, t^{n+1}) 2\pi r\, dr = 2\pi r_i \Delta r_i \tag{A6}$$

so that the test function defines the correct total weighting. Thus with the strategic point approach developed for Cartesian coordinates in the text, which is intended to integrate test functions accurately, we obtain accurate mass distribution and avoid oscillations in radial coordinates as well.

NOTATION

c	concentration (mL^{-3}).
Cr	Courant number.
D	dispersion coefficient (L^2T^{-1}).
f	source/sink ($mL^{-3}T^{-1}$).
h	specified boundary.
i	index for nodes.
L	equation operator.
L	number of cells in spatial grid.
l	length of domain (L).
n	time level.
NS	number of spatial integration points.

NT total number of integration points.
$n(x)$ outward unit normal on $\partial\Omega$.
Pe cell Peclet number.
SSIP strategic spatial integration points.
STIP strategic time integration points.
T final time (T).
t time (T).
t^* time at which spatial integration point is tracked to boundary (T).
U integration weight (L).
v velocity (LT^{-1}).
W_i approximate test function.
w test function.
X tracked location of x (L).
$x_p(t)$ position of integration point at time t (L).
$\hat{x}$ forward tracked location of $x(t^n)$ at t^{n+1} (L).
x^* backtracked location of $x(t^{n+1})$ at t^n (L).
α dispersivity (L).
$\partial\Omega$ domain boundary.
Δx_i grid spacing for cell i (L).
Δt time step size (T).
$\Delta t(x)$ time in which x backtracks to boundary (T).
Ω solution domain.

REFERENCES

Baliga, B. R., and S. V. Patankar, A new finite-element formulation for convection-diffusion problems, *Numer. Heat Transfer, 3*, 393–409, 1980.

Bouloutas, E. T., and M. A. Celia, An analysis of some classes of Petrov-Galerkin and optimal test function methods, in *Proceedings of Seventh International Conference on Computational Methods in Water Resources*, vol. 2, edited by M. A. Celia et al., pp. 15–20, Computational Mechanics Publications, Southampton, England, 1988.

Brooks, A., and T. J. R. Hughes, Streamline upwind Petrov-Galerkin formulations for convection dominated flows with particular emphasis on the incompressible Navier-Stokes equations, *Comput. Methods Appl. Mech. Eng., 32*, 199–259, 1982.

Celia, M. A., T. F. Russell, I. Herrera, and R. E. Ewing, An Eulerian-Lagrangian localized adjoint method for the advection-diffusion equation, *Adv. Water Resour., 13*(4), 187–206, 1990.

Cox, R. A., and T. Nishikawa, A new total variation diminishing scheme for the solution of advective-dominant solute transport, *Water Resour. Res., 27*(10), 2645–2654, 1991.

Dahle, H. K., M. S. Espedal, and R. E. Ewing, Characteristic Petrov-Galerkin subdomain methods for convection diffusion problems, in *Numerical Simulation in Oil Recovery*, edited by M. F. Wheeler, pp. 77–88, Springer-Verlag, New York, 1988.

Douglas, J., Jr., and T. F. Russell, Numerical methods for convection-dominated diffusion problems based on combining the method of characteristics with finite element or finite difference procedures, *SIAM J. Numer. Anal., 19*, 871–885, 1982.

Espedal, M. S., and R. E. Ewing, Characteristic Petrov-Galerkin subdomain methods for two-phase immiscible flow, *Comput. Methods Appl. Mech. Eng., 64*, 113–136, 1987.

Forsyth, P. A., A control volume finite-element method for local mesh refinement, paper SPE 18415, presented at 10th SPE Symposium on Reservoir Simulation, Soc. of Pet. Eng., Dallas, Tex., 1989.

Garder, A. O., D. W. Peaceman, and A. L. Pozzi, Numerical calculations of multidimensional miscible displacement by the method of characteristics, *Soc. Pet. Eng. J., 4*(1), 26–36, 1964.

Gelhar, L. W., and M. A. Collins, General analysis of longitudinal dispersion in nonuniform flow, *Water Resour. Res., 7*(6), 1511–1521, 1971.

Healy, R. W., Simulation of solute transport in variably saturated porous media with supplemental information on modifications to the U.S. Geological Survey's Computer Program VS2D, *U.S. Geol. Surv. Water Resour. Invest., 90-4025*, 125 pp., 1990.

Healy, R. W., and T. F. Russell, Efficient implementation of the modified method of characteristics in finite difference models of solute transport, in *Proceedings of Conference in Solving Ground Water Problems with Models*, edited by J. Lehr, pp. 483–491, National Well Water Association, Indianapolis, Indiana, 1989.

Heinemann, Z. E., C. Brand, M. Munka, and Y. M. Chen, Modeling reservoir geometry with irregular grids, paper SPE 18412, presented at 10th SPE Symposium on Reservoir Simulation, Soc. of Pet. Eng., Dallas, Tex., 1989.

Hoopes, J. A., and D. R. Harleman, Dispersion in radial flow from a recharge well, *J. Geophys. Res., 72*(14), 3595–3607, 1967.

Hsieh, P. A., A new formula for the analytical solution of the radial dispersion problem, *Water Resour. Res., 22*(11), 1597–1605, 1986.

Konikow, L. F., and J. D. Bredehoeft, Computer model of two-dimensional solute transport and dispersion in groundwater, in *Techniques of Water-Resource Investigations*, Book 7, Chapter C2, 90 pp., U.S. Geological Survey, Washington, D. C., 1978.

Liu, C., and S. McCormick, The finite volume element method (FVE) for planar cavity flow, paper presented at 11th International Conference on Numerical Methods in Fluid Dynamics, Univ. of William and Mary, Williamsburg, Va., June 27 to July 1, 1988.

Neuman, S. P., An Eulerian-Lagrangian numerical scheme for the dispersion-convection equation using conjugate space-time grids, *J. Comput. Phys., 41*, 270–294, 1981.

Neuman, S. P., Adaptive Eulerian-Lagrangian finite-element method for advection-dispersion, *Int. J. Numer. Methods Eng., 20*, 321–337, 1984.

Ogata, A., and R. B. Banks, A solution of the differential equation of longitudinal dispersion in porous media, *U.S. Geol. Surv. Prof. Pap., 411-A*, 7 pp., 1961.

Pollock, D. W., Semianalytical computation of path lines for finite-difference models, *Ground Water, 26*(6), 743–750, 1988.

Rozon, B., A generalized finite volume discretization method for reservoir simulation, paper SPE 18414, presented at 10th SPE Symposium on Reservoir Simulation, Soc. of Pet. Eng., Dallas, Tex., 1989.

Russell, T. F., Time stepping along characteristics with incomplete iteration for a Galerkin approximation of miscible displacement in porous media, *SIAM J. Numer. Anal., 22*, 970–1013, 1985.

Russell, T. F., Eulerian-Lagrangian localized adjoint methods for advection-dominated problems, in *Numerical Analysis 1989, Pitman Res. Notes Math. Ser.*, vol. 228, edited by D. F. Griffiths and G. A. Watson, pp. 206–228, Longman Scientific and Technical, Harlow, England, 1990.

Russell, T. F., and R. V. Trujillo, Eulerian-Lagrangian localized adjoint methods with variable coefficients in multiple dimensions, in *Computational Methods in Surface Hydrology: Proceedings of Eighth International Conference on Computational Methods in Water Resources*, edited by G. Gambolati et al., pp. 357–363, Computational Mechanics Publications, Southampton, England, 1990.

Russell, T. F., M. F. Wheeler, and C. Y. Chiang, Large-scale simulation of miscible displacement by mixed and characteristic finite element methods, in *Mathematical and Computational Methods in Seismic Exploration and Reservoir Modeling*, edited by W. E. Fitzgibbon, pp. 85–107, Society for Industrial and Applied Mathematics, Philadelphia, Pa., 1986.

Tang, D. H., and D. K. Babu, Analytical solution of a velocity dependent dispersion problem, *Water Resour. Res., 15*(6), 1471–1478, 1979.

Westerink, J. J., and D. Shea, Consistent higher degree Petrov-Galerkin methods for the solution of the transient convection-diffusion equation, *Int. J. Numer. Method. Eng., 28*, 1077–1101, 1989.

R. W. Healy, Water Resources Division, U.S. Geological Survey, Box 25046, MS 413, Denver Federal Center, Denver, CO 80225.

T. F. Russell, Department of Mathematics, University of Colorado, P.O. Box 173364, Campus Box 170, Denver, CO 80217-3364.

(Received July 10, 1992;
revised February 1, 1993;
accepted February 16, 1993.)